

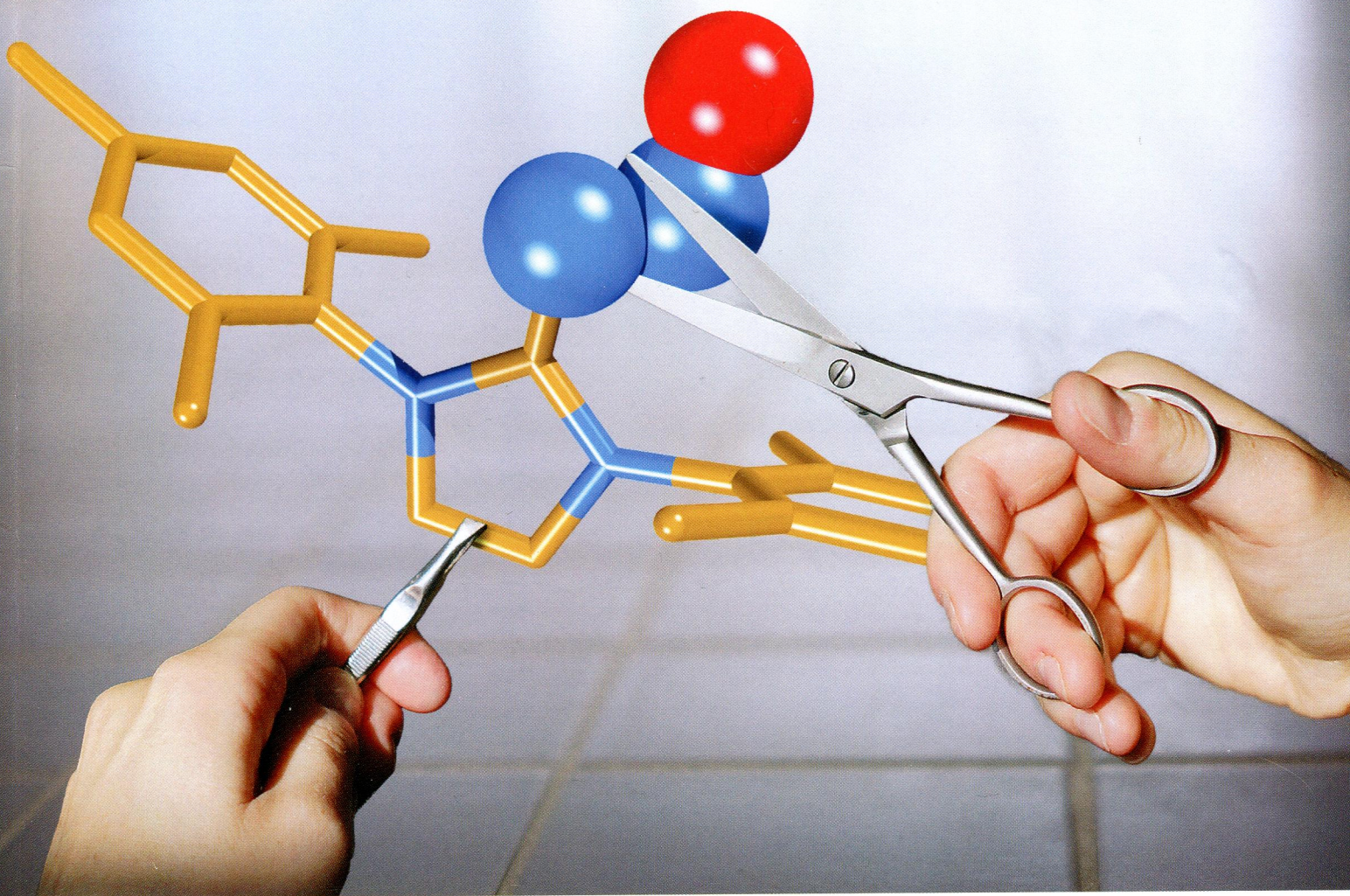
74
I-65

Inorganic Chemistry

including bioinorganic chemistry

October 21, 2013
Volume 52, Number 20
pubs.acs.org/IC

Cutting activated N_2O with a "nickel scissor"



ACS Publications
MOST TRUSTED. MOST CITED. MOST READ.

www.acs.org

ON THE COVER: After activation of nitrous oxide by *N*-heterocyclic carbenes, zerovalent nickel ("the scissor") can insert into the *N*–*N* bond. See A. G. Tskhovrebov, E. Solari, R. Scopelliti, and K. Severin, p 11688.

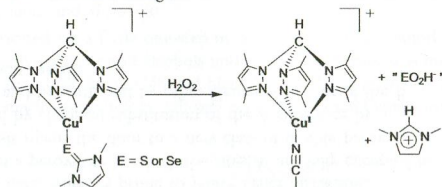
Communications

 11685 **S**
dx.doi.org/10.1021/ic401366c

Oxidation of Biologically Relevant Chalcogenones and Their Cu(I) Complexes: Insight into Selenium and Sulfur Antioxidant Activity

Martin M. Kimani, Craig A. Bayse, Bradley S. Stadelman, and Julia L. Brumaghim*

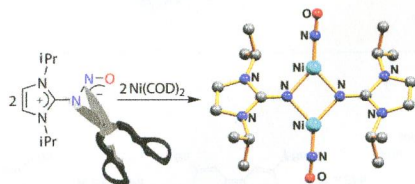
The treatment of copper(I) seleno and thiono complexes with up to 3 equiv of hydrogen peroxide preferentially oxidizes the selenium or sulfur ligand instead of copper(I). This reactivity indicates that metal-bound selenium and sulfur antioxidants may act as targeted scavengers to prevent oxidative damage.


 11688 **S**
dx.doi.org/10.1021/ic401524w

Insertion of Zerovalent Nickel into the *N*–*N* Bond of *N*-Heterocyclic-Carbene-Activated N_2O

Alexander G. Tskhovrebov, Euro Solari, R sario Scopelliti, and Kay Severin*

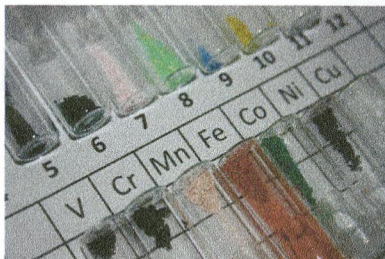
Upon activation of N_2O with *N*-heterocyclic carbenes, zerovalent nickel is able to insert into the *N*–*N* bond to give nitrosyl complexes.



Microwave-Assisted Carbohydrohalogenation of First-Row Transition-Metal Oxides (M = V, Cr, Mn, Fe, Co, Ni, Cu) with the Formation of Element Halides

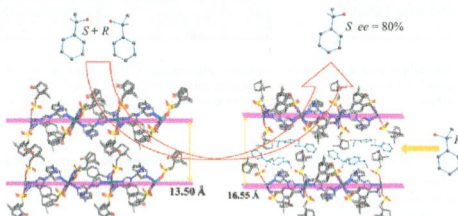
Matthias Berger, Felix Neumeyer, and Norbert Auner*

The anhydrous metal chlorides and bromides ranging from vanadium to copper were synthesized in a one-step microwave reaction using hydrogen halides, graphite, and the corresponding element oxides.

**Enantioselective Recognition and Separation of Racemic 1-Phenylethanol by a Pair of 2D Chiral Coordination Polymers**

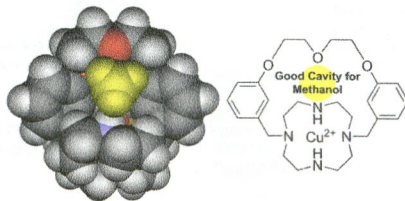
Zi-Jian Li, Jia Yao, Qian Tao, Long Jiang,* and Tong-Bu Lu*

A pair of 2D chiral coordination polymers were constructed, which shows enantioselective separation of racemic 1-phenylethanol, with a selectivity of 9:1 and an e_e value of 80%.

**Selective Retention of Methanol over Ethanol by a Cyclen-Based Cryptand/Copper(II) Complex**

Yoichi Habata,* Mari Ikeda, Ajay K. Sah, Kanae Noto, and Shunsuke Kuwahara

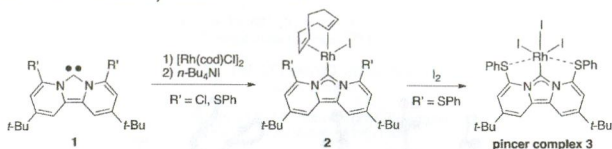
A cyclen-based cryptand (**2**) has been prepared. When the $\text{Cu}(\text{CF}_3\text{SO}_3)_2$ complex with **2** was prepared in methanol, one methanol was included in the three-dimensional cavity formed by the diethyleneoxy unit and the NH group of the cyclen. When formed in ethanol, the $\text{2}/\text{Cu}(\text{CF}_3\text{SO}_3)_2$ complex included ethanol. Cold electrospray ionization mass spectrometry (CSI-MS) of the complexes reveals that the $\text{2}/\text{Cu}(\text{CF}_3\text{SO}_3)_2$ complex retains both methanol and ethanol under CSI-MS conditions.



Synthesis of New Dipyrido-Annulated N-Heterocyclic Carbenes with Ortho Substituents

Shin-ichi Fuku-en, Junki Yamamoto, Mao Minoura, Satoshi Kojima, and Yohsuke Yamamoto*

A simple method for synthesizing new dipyrido-annulated N-heterocyclic carbene ligands **1** bearing ortho substituents R' (R' = Cl, SPh) was developed. The reaction of rhodium(I) with the in situ generated carbenes **1** furnished the corresponding carbenerhodium(I) complexes **2**. In the case of **2** bearing sulfur substituents, the first carbene-centered pincer complex **3** (R' = SPh) with a fixed scaffold was obtained by oxidation with iodine.



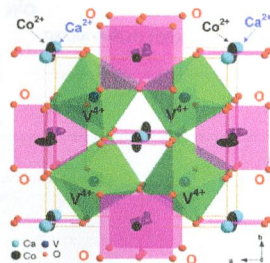
Articles

New Antiferromagnetic Perovskite CaCo₃V₄O₁₂ Prepared at High-Pressure and High-Temperature Conditions

Sergey V. Ovsyannikov,* Yury G. Zainulin, Nadezda I. Kadyrova, Alexander P. Tyutyunnik, Anna S. Semenova, Deepa Kasinathan, Alexander A. Tsrilin, Nobuyoshi Miyajima, and Alexander E. Karkin

We report a high-pressure and high-temperature synthesis of a new double perovskite, CaCo²⁺₃V⁴⁺₄O₁₂, crystallizing in a cubic structure. CaCo₃V₄O₁₂ orders antiferromagnetically around 98 K. We found that the Co²⁺ ions in CaCo₃V₄O₁₂ are in the high-spin state with a sizable orbital moment, even though their square-planar oxygen coordination could be more suitable for a low-spin state, which is prone to Jahn–Teller distortion.

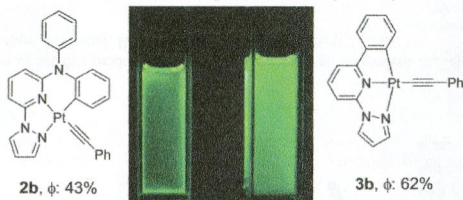
CaCo₃V₄O₁₂ is a first example of a perovskite in which the sites A' are fully occupied by Co²⁺ ions, and hence its synthesis opens the door to a new class of double perovskites, ACo₃B₄O₁₂, that may be derived by chemical substitution of the A sublattice by lanthanides, sodium, strontium, and bismuth and by other elements and/or of the B sublattice by some other transition metals.



Synthesis, Structure, Photophysics, and a DFT Study of Phosphorescent C*N^N- and C^N^N-Coordinated Platinum Complexes

Caleb F. Harris, Dileep A. K. Vezzu, Libero Bartolotti, Paul D. Boyle, and Shouquan Huo*

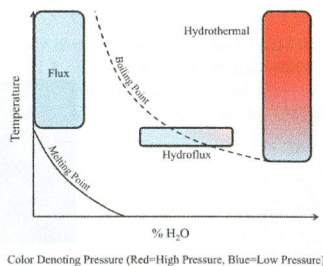
The C*N^N- and C^NN-coordinated platinum complexes have been synthesized, and their structural and photophysical properties have been investigated. Two cyclometalated platinum complexes based on *N,N*-diphenyl-6-(1*H*-pyrazol-1-yl)pyridin-2-amine (C*N^N) and 2-phenyl-6-(1*H*-pyrazol-1-yl)pyridine (C^NN) ligands are highly emissive at ambient temperature in solution. The use of pyrazolylpyridine as the N^N motif seems critical to achieving the high efficiency of green light emission. When bipyridine was used instead, the complexes were only weakly emissive in the orange to red region.



Crystal Growth of New Hexahydroxometallates Using a Hydroflux

W. Michael Chance, Daniel E. Bugaris, Athena S. Sefat, and Hans-Conrad zur Loye*

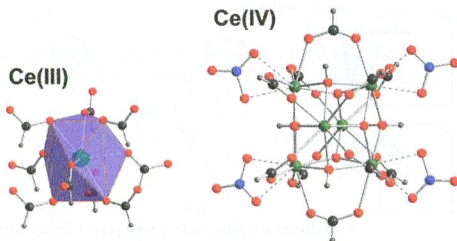
A series of new hexahydroxometallates of the type $A_2B(OH)_6$, where $A = Sr, Ba$ and $B = Mn, Co, Ni, Cu$, were synthesized using a hydroxide-based hydroflux, a hybrid approach that combines hydrothermal and molten hydroxide flux techniques. Very little pressure is generated, and the reactions, which yield high-quality single crystals, are complete in less than 1 day.



Crystal Structure and Solution Species of Ce(III) and Ce(IV) Formates: From Mononuclear to Hexanuclear Complexes

Christoph Hennig,* Atsushi Ikeda-Ohno, Werner Kraus, Stephan Weiss, Philip Pattison, Hermann Emerich, Paula M. Abdala, and Andreas C. Scheinost

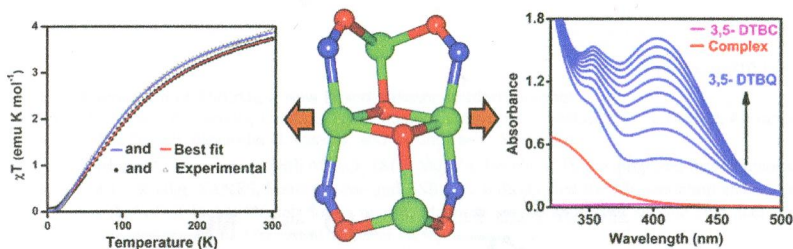
Cerium(III) and cerium(IV) both form formate complexes. However, the species in aqueous solution and the solid-state structures are surprisingly different. Ce(III) shows only mononuclear complexes in aqueous solution, whereas Ce(IV) forms a stable hexanuclear complex. The structural differences reflect the different influence of hydrolysis, which is weak for Ce(III) and strong for Ce(IV).



Di-, Tri-, and Tetranuclear Nickel(II) Complexes with Oximate Bridges: Magnetism and Catecholase-like Activity of Two Tetranuclear Complexes Possessing Rhombic Topology

Lakshmi Kanta Das, Apurba Biswas, Jared S. Kinyon, Naresh S. Dalal,* Haidong Zhou, and Ashutosh Ghosh*

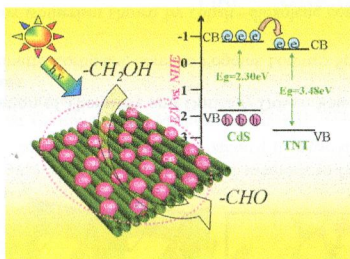
One dinuclear, one trinuclear, and two rhombic tetranuclear nickel(II) complexes have been synthesized using two tridentate Schiff base ligands depending upon the reaction conditions and chelating ring size of the ligand moiety. Both of the tetranuclear complexes exhibit dominant antiferromagnetic intramolecular coupling with concomitant ferromagnetic interactions as well as excellent catalytic activity in the areal oxidation of 3,5-di-*tert*-butylcatechol to the corresponding *o*-quinone.



Synthesis of Titanate Nanotube–CdS Nanocomposites with Enhanced Visible Light Photocatalytic Activity

Zi-Rong Tang,* Xia Yin, Yanhui Zhang, and Yi-Jun Xu

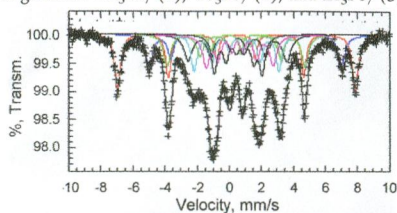
CdS/TNTs nanocomposites fabricated via a facile one-step in situ hydrothermal method are used as a visible light photocatalyst toward aerobic selective oxidation of alcohols under mild conditions. It is found that CdS/TNTs exhibit much higher visible light photoactivity than both blank-CdS and blank-TNT. The improved photocatalytic performance of CdS/TNTs can be attributed to their specific morphology, efficient separation of photogenerated charge carriers, and high surface area and adsorption capacity.



Synthesis, Magnetism, and ^{57}Fe Mössbauer Spectroscopic Study of a Family of $[\text{Ln}_3\text{Fe}_7]$ Coordination Clusters (Ln = Gd, Tb, and Er)

Ghulam Abbas, Yanhua Lan, Valeriu Mereacre, Gernot Buth, Moulay T. Sougrati, Fernande Grandjean, Gary J. Long,* Christopher E. Anson, and Annie K. Powell*

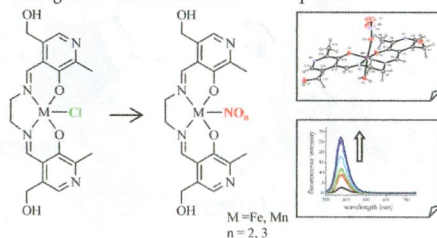
A transmission versus velocity plot is given for Gd_3Fe_7 (1), Tb_3Fe_7 (2), and Er_3Fe_7 (3).



Iron and Manganese Pyridoxal-Based Complexes as Fluorescent Probes for Nitrite and Nitrate Anions in Aqueous Solution

Maria Strianese, Stefano Milione,* Valerio Bertolasi, and Claudio Pellicchia

We devised new iron and manganese pyridoxal-based complexes for the selective fluorescent detection of nitrite and nitrate in water solution. The addition of nitrite or nitrate anion to a water solution of the title complexes results in the chloride displacement, causing an increase in fluorescence emission. The present data provide proof-of-principle that it is possible to monitor weak coordinating anions using metal-based coordination complexes.

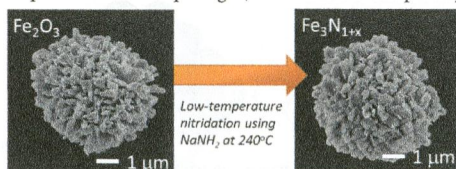


Turn-ON fluorescence response in water solution

Low-Temperature Nitridation of Manganese and Iron Oxides Using NaNH_2 Molten Salt

Akira Miura,* Takahiro Takei, and Nobuhiro Kumada

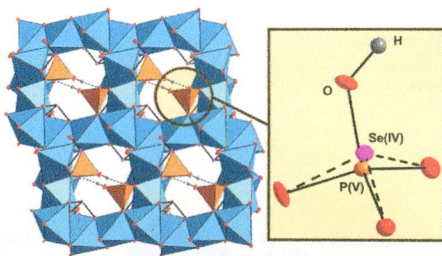
Manganese and iron nitrides are important functional materials, but their synthesis processes from oxides often require high temperatures. Herein, we show a novel meta-synthesis method for manganese and iron nitrides by low-temperature nitridation of their oxides using NaNH_2 molten salt as the nitrogen source in an autoclave at 240 °C. With this method, nitridation of micrometer-sized oxide particles kept their initial morphologies, but the size of the primary particles decreased.



Synthesis and Crystal Structure of the Solid Solution $\text{Co}_3(\text{SeO}_3)_{3-x}(\text{PO}_3\text{OH})_x(\text{H}_2\text{O})$ Involving Crystallographic Split Positions of Se^{4+} and P^{5+}

Iwan Zimmermann and Mats Johnson*

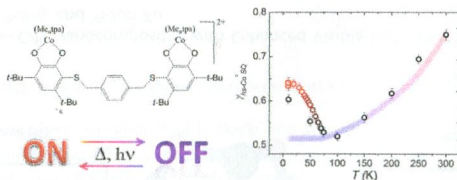
The solid solution $\text{Co}_3(\text{SeO}_3)_{3-x}(\text{PO}_3\text{OH})_x(\text{H}_2\text{O})$ exhibits an unusual mixed position of $\text{Se}(\text{IV})$ and $\text{P}(\text{V})$. Three compounds with $x = 0.8$, $x = 1.0$, and $x = 1.2$, respectively, have been characterized by means of X-ray diffraction, magnetic measurements, IR, TG, and EDS. The compound undergoes antiferromagnetic ordering below 16 K and a magnetic moment of $4.02(3) \mu_{\text{B}}$ per Co atom was observed. The release of the crystal water occurs at such a high temperature, above 450°C , due to the presence of hydrogen bonds.



Magnetic and Spectroscopic Investigation of Thermally and Optically Driven Valence Tautomerism in Thioether-Bridged Dinuclear Cobalt–Dioxolene Complexes

Giordano Poneti,* Matteo Mannini, Brunetto Cortigiani, Lorenzo Poggini, Lorenzo Sorace, Edwige Otero, Philippe Saintavirt, Roberta Sessoli, and Andrea Dei

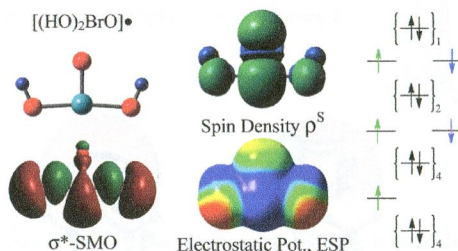
The light- and temperature-driven redox isomerism shown by cobalt–dioxolene complexes makes them potential building blocks for application in nanosized spintronics and sensor devices. In this work we report the functionalization of the dioxolene ring with a thioether bridge to obtain the dinuclear molecular species $[\text{Co}(\text{Me}_n\text{tpa})\text{-diox-S-diox-Co}(\text{Me}_n\text{tpa})]-(\text{PF}_6)_2$. Magnetometric, X-ray photoelectron spectroscopy, and X-ray absorption spectroscopy revealed that the functionalization preserved the coordination properties of the dioxolene ligand and the thermal and optical switchability of one of its complexes.



Electronic Structures and Spin Density Distributions of BrO₂ and (HO)₂BrO Radicals. Mechanisms for Avoidance of Hypervalency and for Spin Delocalization and Spin Polarization

Rainer Glaser* and Cory Camasta

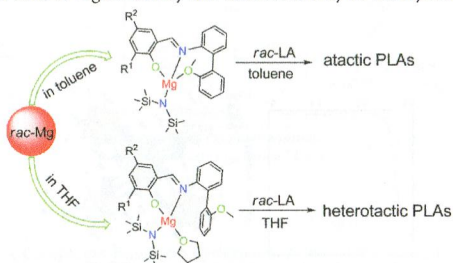
Spin density distributions and molecular electrostatic potentials were computed at highly correlated levels to characterize the electronic structures of BrO₂, **1**, and of the T-shaped trans- and cis-dihydroxides **2** and **3** of (HO)₂BrO. Molecular orbital theory is employed to describe the mechanisms for the avoidance of hypervalency and for spin delocalization and spin polarization. The (4c-7e) π -system in **2** is truly remarkable in that it contains five π -symmetric spin molecular orbitals (SMO) with unique shapes.



Magnesium and Calcium Complexes Containing Biphenyl-Based Tridentate Iminophenolate Ligands for Ring-Opening Polymerization of *rac*-Lactide

Wei Yi and Haiyan Ma*

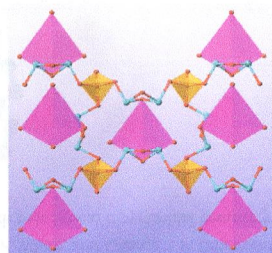
Biphenyl-based tridentate magnesium and calcium iminophenolate complexes efficiently catalyzed the ring-opening polymerization of *rac*-lactide and showed higher activity and stereoselectivity in tetrahydrofuran than in toluene.



Ba₁₃Si₆Sn₈As₂₂: A Quaternary Zintl Phase Containing Adamantane-Like [Si₄As₁₀] Clusters

Xiao-Cun Liu, Na Lin, Jian Wang, Ming-Yan Pan, Xian Zhao, Xu-Tang Tao, and Sheng-Qing Xia*

A new quaternary Zintl phase, Ba₁₃Si₆Sn₈As₂₂, is synthesized from Sn-flux reactions. Its anionic structure can be described as composed of adamantane-like [Si₄As₁₀] clusters and SiAs₄ tetrahedral units, which are interlinked through the [Sn₂As₄] groups. Both optical absorption spectrum and theoretical calculations indicate that Ba₁₃Si₆Sn₈As₂₂ is a small band gap semiconductor. With the existence of lone pair electrons on the *p*-orbitals of Sn and As, interesting NLO properties may be expected.



More on Diphosphadithiatetrazocines and the Importance of Being Bonded

Heiko Jacobsen*

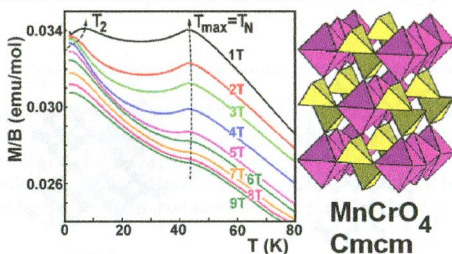
The putative cross-ring sulfur–sulfur bond in diphosphadithiatetrazocines is investigated by a fragment-based bond energy determination, and by a topology analysis of a bond descriptor based on the local kinetic energy density.



Synthesis and Characterization of MnCrO_4 , a New Mixed-Valence Antiferromagnet

Vladimir B. Nalbandyan,* Elena A. Zvereva, Galina E. Yalovega, Igor L. Shukaev, Anastasiya P. Ryzhakova, Alexander A. Guda, Alessandro Stroppa, Silvia Picozzi, Alexander N. Vasiliev, and Myung-Hwan Whangbo

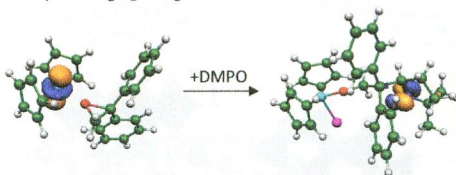
Black semiconducting MnCrO_4 , isostructural with MCrO_4 ($M = \text{Mg}, \text{Co}, \text{Ni}, \text{Cu}, \text{Cd}$), was prepared from aqueous precursors at 400°C . The Mn and Cr K edge XANES, bond valence and ESR data indicate that the Mn oxidation state is considerably higher than 2, whereas that of Cr is considerably lower than 6. Magnetic susceptibility and specific heat data supported by DFT calculations indicate occurrence of a 3D AFM order at ca. 42 K.



Radical-Based Epoxide Opening by Titanocenes

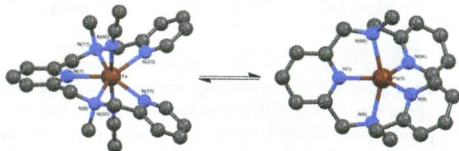
Asli Cangönül, Maike Behlendorf, Andreas Gansäuer,* and Maurice van Gestel*

Titanocene-mediated radical-based opening of epoxides has been studied by EPR spectroscopy and quantum chemistry. A radical intermediate has been trapped and identified by spin-trapping methods to provide a first, complete, *experimentally verified* picture of the titanocene-catalyzed ring-opening reaction.



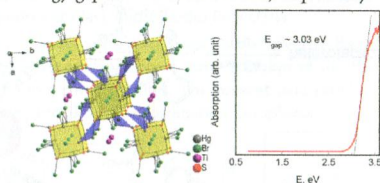
Coordination Equilibria Between Seven- and Five-coordinate Iron(II) Complexes

Michaela Grau, Jason England, Rafael Torres Martin de Rosales, Henry S. Rzepa, Andrew J. P. White, and George J. P. Britovsek*
 First observations of dynamic equilibria between seven-coordinate iron(II) complexes with pentagonal bipyramidal geometry and five-coordinate iron(II) complexes with trigonal bipyramidal geometry.

**Thallium Mercury Chalcobromides, $\text{TlHg}_6\text{Q}_4\text{Br}_5$ (Q = S, Se)**

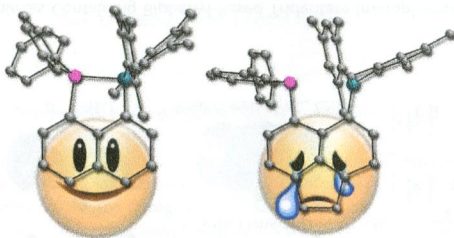
Arief C. Wibowo, Christos D. Malliakas, Duck Young Chung, Jino Im, Arthur J. Freeman, and Mercurio G. Kanatzidis*

$\text{TlHg}_6\text{S}_4\text{Br}_5$ and $\text{TlHg}_6\text{Se}_4\text{Br}_5$ are novel compounds, with unusual three-dimensional structures of high symmetry ($I4/m$), high specific density ($>7 \text{ g/cm}^3$), and wide energy gaps of 3.03 and 2.80 eV, respectively.

**Peri-Substituted (Ace)Naphthylphosphinoboranes. (Frustrated) Lewis Pairs**

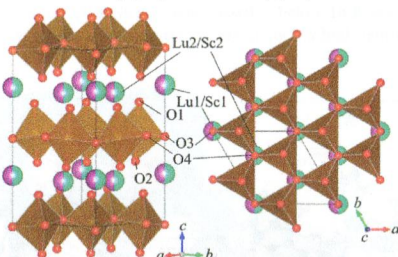
Jens Beckmann,* Emanuel Hupf, Enno Lork, and Stefan Mebs*

The closely related title compounds possess quite different P–B *peri* distances of 2.162(2) and 3.050(3) Å, which allow them to be classified as regular and frustrated Lewis pairs.



Weak Ferromagnetic Transition with a Dielectric Anomaly in Hexagonal $\text{Lu}_{0.5}\text{Sc}_{0.5}\text{FeO}_3$

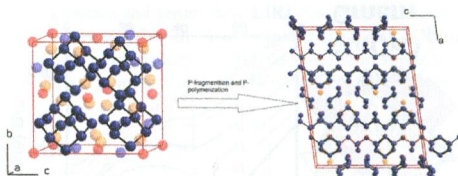
Atsunobu Masuno,* Atsushi Ishimoto, Chikako Moriyoshi, Naoaki Hayashi, Hitoshi Kawaji, Yoshihiro Kuroiwa, and Hiroyuki Inoue
Hexagonal $\text{Lu}_{0.5}\text{Sc}_{0.5}\text{FeO}_3$ has been prepared by conventional solid-state reactions. Rietveld analysis using synchrotron X-ray diffraction data demonstrated that the space group is $P6_3cm$ as well as ferroelectric hexagonal RMnO_3 and the crystal structure is hexagonal with unit cell parameters $a = 5.86017(7)$ Å, $c = 11.7105(2)$ Å, and $Z = 6$.



Temperature Initiated P-Polymerization in Solid $[\text{Cd}_3\text{Cu}]_n\text{CuP}_{10}$

Melanie Bawohl, Peer Schmidt,* and Tom Nilges*

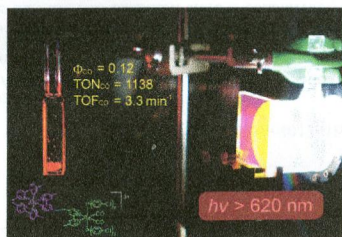
$[\text{Cd}_3\text{Cu}]_n\text{CuP}_{10}$ is the first representative of a class of compounds featuring polyphosphidic adamantane-analogous $[\text{P}_{10}]$ units, which tend to be fragmented and polymerized to $[\text{P}_6]$ rings and tubular $[\text{P}_{26}]$ units in the solid state. A new polyphosphide with nominal composition $\text{Cd}_{15}\text{Cu}_{10}\text{P}_{46}$ results, featuring isolated and polymerized polyanions. Thermoanalytic experiments and phase analytic measurements substantiated the consecutive loss of P_4 and Cd of the starting material via different intermediate steps. After P_4 loss, the new polyphosphide occurred followed by various binary copper phosphides to the final product Cu_3P .



Red-Light-Driven Photocatalytic Reduction of CO_2 using $\text{Os(II)}-\text{Re(I)}$ Supramolecular Complexes

Yusuke Tamaki, Kazuhide Koike, Tatsuki Morimoto, Yasuomi Yamazaki, and Osamu Ishitani*

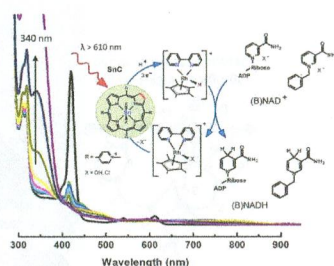
Novel $\text{Os(II)}-\text{Re(I)}$ supramolecular photocatalysts were developed. They photocatalyzed CO_2 reduction selectively to CO with relatively high efficiency, durability, and rate under red-light irradiation.



Photocatalytic Reduction of Artificial and Natural Nucleotide Co-factors with a Chlorophyll-Like Tin-Dihydroporphyrin Sensitizer

Kerstin T. Oppelt, Eva Wöfl, Martin Stifinger, Wolfgang Schöfberger, Wolfgang Buchberger, and Günther Knör*

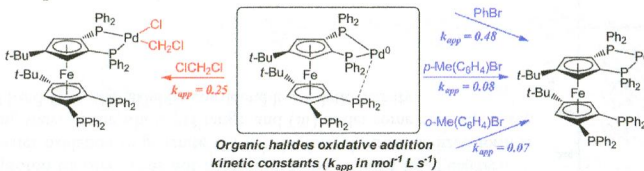
An efficient photocatalytic system for the two-electron reduction of nucleotide co-factors has been characterized. For the first time it could be demonstrated in an abiotic system that the long-wavelength region of the visible spectrum (> 610 nm) can be exploited to power the accumulation of NADH. The artificial photosynthetic reaction sequence, described here in detail, can be regarded as the first true functional model system for the overall light reactions occurring in natural photosystem I.



Kinetic and Electrochemical Studies of the Oxidative Addition of Demanding Organic Halides to Pd(0): the Efficiency of Polyphosphane Ligands in Low Palladium Loading Cross-Couplings Decrypted

Veronika A. Zinovyeva, Sopal Mm, Sophie Fournier, Charles H. Devillers, H el ene Cattey, Henri Doucet, Jean-Cyrille Hierso,* and Dominique Lucas*

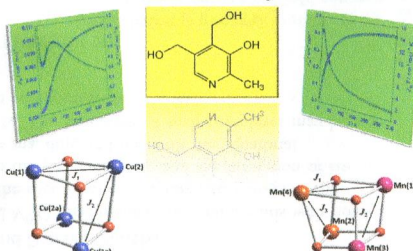
Cyclic voltammetry allowed measuring and comparing the rate of the oxidative addition (OA) of organic halides to Pd(0) complexes coordinated by ferrocenyl di-, tri-, and tetraphosphane ligands of related structures. The influence of the phosphane features on the intermediates formed, on the rates of OA, and also on the stereoselectivity of the reaction was investigated by electroanalysis. The straightforward electrosynthesis of some OA products was achieved, and the X-ray structure of an elusive alkyl Pd(II)chloro complex was resolved.



Cubane-Type Cu^{II}_4 and $\text{Mn}^{\text{II}}_2\text{Mn}^{\text{III}}_2$ Complexes Based on Pyridoxine: A Versatile Ligand for Metal Assembling

Nadia Marino, Donatella Armentano,* Teresa F. Mastropietro, Miguel Julve, Giovanni De Munno, and Jos e Mart inez-Lillo*

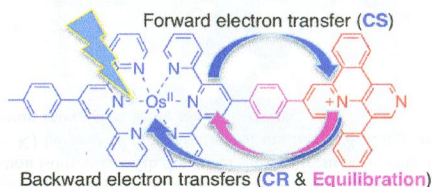
Two tetranuclear Cu^{II}_4 and $\text{Mn}^{\text{II}}_2\text{Mn}^{\text{III}}_2$ compounds of formula $[\text{Mn}_4(\text{PN-H})_4(\text{CH}_3\text{CO}_2)_3\text{Cl}_2]\text{Cl}\cdot 2\text{CH}_3\text{OH}\cdot 2\text{H}_2\text{O}$ (1) and $[\text{Cu}_4(\text{PN-H})_4\text{Cl}_2(\text{H}_2\text{O})_2]\text{Cl}_2$ (2) have been synthesized and magneto-structurally characterized by using Vitamin B₆ in its monodeprotonated pyridoxine form (PN-H) [PN = 3-hydroxy-4,5-bis(hydroxymethyl)-2-methylpyridine] as ligand. Both compounds show behavior typical of antiferromagnetically coupled systems exhibiting susceptibility maxima at 5 (1) and 65 K (2), and their experimental magnetic data have been modeled through Hamiltonians with three (1) and two (2) *J* values.



Molecular Dyads of Ruthenium(II)– or Osmium(II)–Bis(terpyridine) Chromophores and Expanded Pyridinium Acceptors: Equilibration between MLCT and Charge-Separated Excited States

Jérôme Fortage, Grégory Dupeyre, Fabien Tuyères, Valérie Marvaud, Philippe Ochsenbein, Ilaria Ciofini, Magdaléna Hromadová, Lubomír Pospíšil, Antonino Arrigo, Emanuela Trovato, Fausto Puntoriero,* Philippe P. Lainé,* and Sebastiano Campagna*

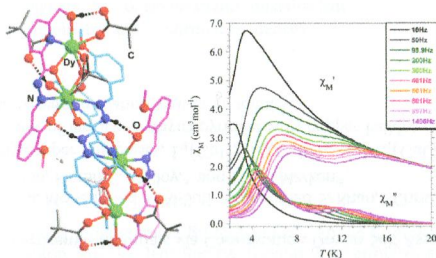
A series of molecular dyads based on Ru(II)– or Os(II)–bis(terpyridine) chromophores and expanded pyridinium acceptors has been prepared. In most dyads, the ³MLCT state and the charge-separated state (formed via photoinduced electron transfer from the MLCT level) are close in energy so that an excited-state equilibration can take place. The effects of such excited-state equilibration on the dyads' photophysical properties, including apparent charge separation and recombination rate constants, are discussed.



Tetranuclear Lanthanide (III) Complexes Containing Dimeric Subunits: Single-Molecule Magnet Behavior for the Dy₄ Analogue

Vadapalli Chandrasekhar,* Sourav Das, Atanu Dey, Sakiat Hossain, and Jean-Pascal Sutter*

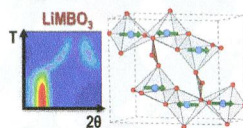
Keto–enol tautomerism and conformational flexibility present in a ligand have been successfully utilized to construct a series of tetranuclear lanthanide complexes [Ln₄(LH)₂(LH₂)₂(μ₂-η¹η¹Piv)₂(η¹Piv)₄].2CHCl₃ [Ln = Dy(1), Tb(2), and Gd(3)] that contain interconnected dimeric subunits. Detailed magnetic studies on 1–3 reveal a SMM behavior for complex 1 with a two-step relaxation, having the energy barriers and relaxation times: Δ/k_B = 62.6 K, τ₀ = 8.7 × 10⁻⁷; Δ/k_B = 26.3 K, τ₀ = 1.26 × 10⁻⁶.



Magnetic Structures of LiMBO₃ (M = Mn, Fe, Co) Lithiated Transition Metal Borates

Liang Tao, James R. Neilson, Brent C. Melot, Tyrel M. McQueen, Christian Masquelier, and Gwenaëlle Rousse*

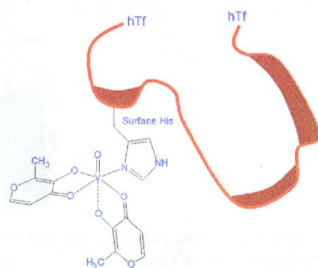
Magnetization measurements and neutron powder diffraction reveal incommensurate and then commensurate long-range antiferromagnetic ordering below 12 K for LiCoBO₃ and LiMnBO₃, and below 25 K for LiFeBO₃. Uncommon trigonal bipyramidal environments can give rise to novel electronic and magnetic phenomena.



Interaction of Insulin-Enhancing Vanadium Compounds with Human Serum holo-Transferrin

Daniele Sanna, Giovanni Micera, and Eugenio Garribba*

The interaction of $V^{IV}O^{2+}$ ion and $V^{IV}O$ insulin-enhancing compounds with holo-hTf (saturated with Fe^{3+} ions in the specific metal binding sites) suggests the presence of nonspecific sites C on the protein surface and the formation of $cis-VOL_2$ (holo-hTf) species, with L = ma, dhp, and pic, with the equatorial coordination of an accessible His-N. The formation of such complexes may be a way for the transport of vanadium compounds in the cells.



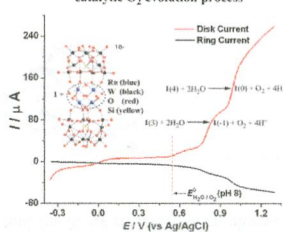
11986

dx.doi.org/10.1021/ic401748y

Voltammetric Determination of the Reversible Potentials for $[(Ru_4O_4(OH)_2(H_2O)_4)(\gamma-SiW_{10}O_{36})_2]^{10-}$ over the pH Range of 2–12: Electrolyte Dependence and Implications for Water Oxidation Catalysis

Yuping Liu, Si-Xuan Guo, Alan M. Bond,* Jie Zhang,* Yurii V. Geletii,* and Craig L. Hill

Analysis of extensive voltammetric data obtained for the water oxidation catalyst $[(Ru_4O_4(OH)_2(H_2O)_4)(\gamma-SiW_{10}O_{36})_2]^{10-}$ in aqueous media over the pH range of 2–12 suggests that (i) proton transfer needs not necessarily be coupled to all electron transfer steps in water oxidation to generate O_2 , (ii) the four-electron oxidized form is capable of oxidizing water in the whole pH range, and (iii) under some conditions, the three-electron oxidized form also exhibits considerable catalytic activity.

Rotating Ring Disk electrode monitoring of catalytic O_2 evolution process

11997

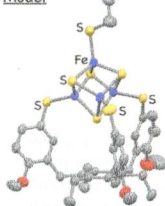
dx.doi.org/10.1021/ic4017596

[3:1] Site-Differentiated [4Fe–4S] Clusters Having One Carboxylate and Three Thiolates

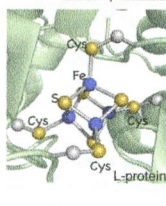
Tamaki Terada, Kiyohisa Hirabayashi, Dong Liu, Tomohiko Nakamura, Takuya Wakimoto, Tsuyoshi Matsumoto,* and Kazuyuki Tatsumi*

[4Fe–4S] Clusters modeled after those in organisms having three cysteine thiolates and one carboxylate were synthesized by using the tridentate thiolato chelate.

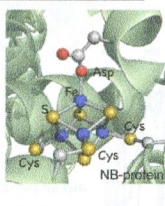
Model



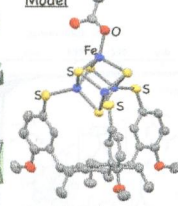
Dark operative protochlorophyllide oxidoreductase



electron transfer



Model



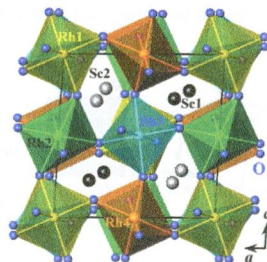
12005 

dx.doi.org/10.1021/ic401760m

High-Pressure Synthesis, Crystal Structures, and Properties of ScRhO₃ and InRhO₃ Perovskites

Alexei A. Belik,* Yoshitaka Matsushita, Masahiko Tanaka, and Eiji Takayama-Muromachi

There has been increased interest in recent years in highly distorted or exotic perovskites in order to find new physical properties, effects, and unusual behavior. We prepared InRhO₃ and a new perovskite ScRhO₃ and investigated their structural and magnetic properties. Both samples have a rarely observed monoclinic superstructure with GdFeO₃-type structure. InRhO₃ and ScRhO₃ are nonmagnetic and have no phase transition between 2 and 873 K.

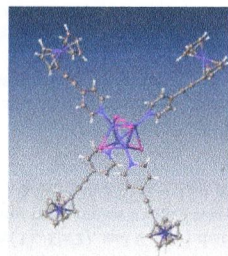

12012 

dx.doi.org/10.1021/ic401803p

New Multi-Ferrocenyl- and Multi-Ferricenyl- Materials via Coordination-Driven Self-Assembly and via Charge-Driven Electro-Crystallization

Hakikulla H. Shah, Rayya A. Al-Balushi, Mohammed K. Al-Suti, Muhammad S. Khan,* Christopher H. Woodall, Anna L. Sudlow, Paul R. Raithby,* Gabriele Kociok-Köhn, Kieran C. Molloy,* and Frank Marken*

The tetra-ferrocenylethynylpyridinylcopper complexes, L₄(CuI)₄, L₄(CuBr)₂, and L₄(CuCl)₂ have been prepared from the reaction of ferrocenylethynylpyridine with copper halides and show chemically reversible multiferrocenyl oxidation signals in solution.

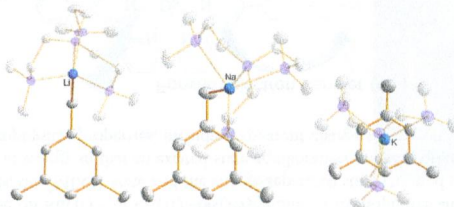
12023 

dx.doi.org/10.1021/ic401777x

Monomerizing Alkali-Metal 3,5-Dimethylbenzyl Salts with Tris(*N,N*-dimethyl-2-aminoethyl)amine (Me₆TREN): Structural and Bonding Implications

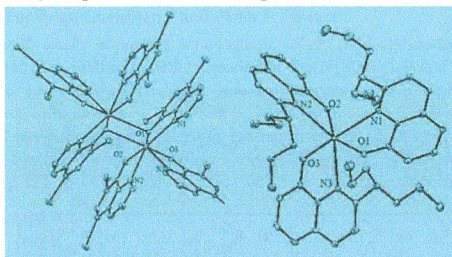
David R. Armstrong, Matthew G. Davidson, Daniel Garcia-Vivo, Alan R. Kennedy, Robert E. Mulvey, and Stuart D. Robertson*

A series of 3,5-dimethylbenzyl alkali-metal complexes (Me₂C₆H₃CH₂M; M = Li, Na, K) have been prepared as stabilized monomers which display coordination isomerism, with the metal slipping from occupying a typical σ -bound position (M = Li) to a more π bound position (M = K) because of delocalization of the negative charge into the aromatic ring. Theoretical calculations show the metal-carbanion interaction to be ionic in nature.



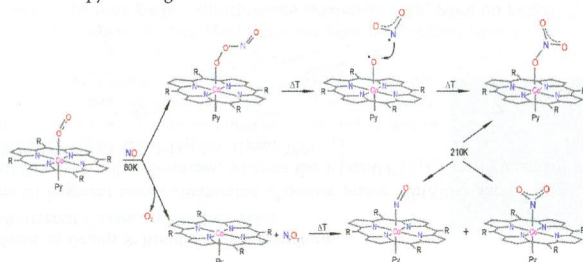
Luminescent Tris(8-hydroxyquinolates) of Bismuth(III)

Pauline J. Han, Arnold L. Rheingold,* and William C. Trogler*

Luminescent Bi(8-hydroxyquinolate)₃ complexes exhibit a facile equilibrium between monomer and dimer forms in solution.**Nitric Oxide Interaction with Oxy-Coboglobin Models Containing *trans*-Pyridine Ligand: Two Reaction Pathways**

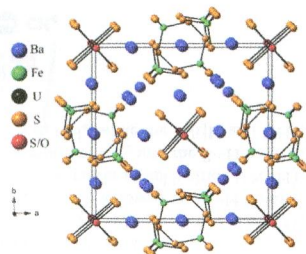
Tigran S. Kurtikyan,* Shahane R. Eksuzyan, John A. Goodwin, and Gohar Sh. Hovhannisyann

NO reacts at low temperatures with layered oxy-coboglobin model compounds, (Py)Co(Por)(O₂), giving the six-coordinate nitrate complexes (Py)Co(Por)(¹η-ONO₂) via initial formation of the six-coordinate peroxyxynitrite complex (Py)Co(Por)(η¹-OONO). Simultaneously due to weak binding some O₂ is released from the parent adduct leading to NO autoxidation and formation of the N_xO_y species in the layer. As a result together with nitrate complexes some quantities of six-coordinate nitro and nitrosyl complexes with *trans*-pyridine ligand are also formed.

**The Flexible Ba₇UM₂S_{12.5}O_{0.5} (M = V, Fe) Compounds: Syntheses, Structures and Spectroscopic, Resistivity, and Electronic Properties**

Adel Mesbah, Wojciech Stojko, Christos D. Malliakas, Sébastien Lebègue, Nicolas Clavier, and James A. Ibers*

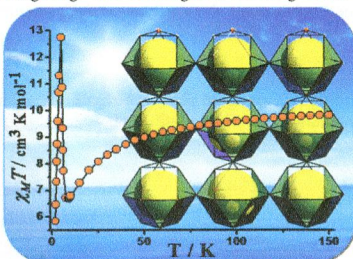
Two new solid-state compounds, Ba₇UV₂S_{12.5}O_{0.5} and Ba₇UF₂S_{12.5}O_{0.5}, have been synthesized at 1223 K. Their structures feature V/S or Fe/S networks and infinite linear US₂O chains. Ba₇UV₂S_{12.5}O_{0.5} contains V⁴⁺, whereas Ba₇UF₂S_{12.5}O_{0.5} contains S₂²⁻ and Fe³⁺. The overall structural motif offers remarkable flexibility in terms of the oxidation state of the incorporated transition metal.



A 3D Iron(II)-Based MOF with Squashed Cuboctahedral Nanoscopic Cages Showing Spin-Canted Long-Range Antiferromagnetic Ordering

Soumyabrata Goswami, Amit Adhikary, Himanshu Sekhar Jena, Soumava Biswas, and Sanjit Konar*

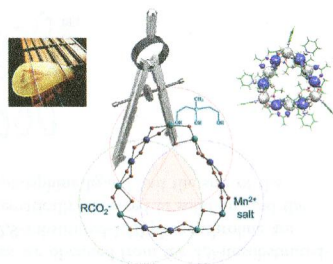
The present work discusses on the synthesis and characterization of an unprecedented 3D Fe(II) MOF with cuboctahedral nanoscopic cages showing spin canted long-range antiferromagnetic ordering in the low temperature region.



A Mn^{II}₆Mn^{III}₆ Single-Strand Molecular Wheel with a Reuleaux Triangular Topology: Synthesis, Structure, Magnetism, and DFT Studies

Sotiris Zartilas, Constantina Papatrifiantylopoulou, Theocharis C. Stamatatos, Vassilios Nastopoulos, Eduard Cremades, Eliseo Ruiz, George Christou, Christos Lampropoulos, and Anastasios J. Tasiopoulos*

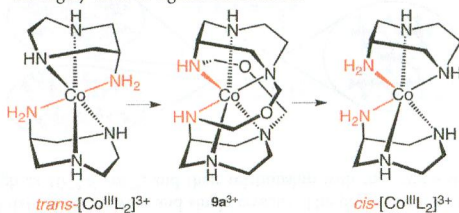
The use of 3-methyl-1,3,5-pentanetriol (H₃mpt) in manganese carboxylate chemistry has afforded a new [Mn^{II}₆Mn^{III}₆(mpt)₆(CH₃CO₂)₁₂(py)₆]_n wheel, with a metal core resembling a guitar plenum. This is the first Mn^{II}₆Mn^{III}₆ wheel made of repeating homovalent dimers and the first example of such a loop with the trigonal symmetry of a Reuleaux triangle, the simplest Reuleaux polygon. It is also a new example of an antiferromagnetic *S* = 0, single-strand, mixed-valent Mn₁₂ wheel, as evidenced from magnetometry and confirmed by density functional theory calculations.



Formation and Base Hydrolysis of Oxidimethanamine Bridges in Co^{III}-Amine Complexes

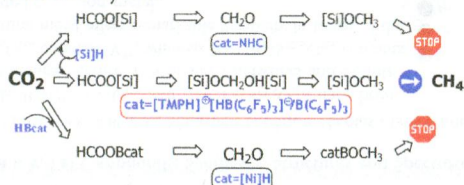
Bernd Morgenstern, Christian Neis, Anton Zschka, Jens Romba, Thomas Weyhermüller, and Kaspar Hegetschweiler*

trans-[Co^{III}L₂]³⁺ reacts in an alkaline, nonaqueous medium with paraformaldehyde to *cis*-configured, dibridged **9a**³⁺, which in turn degrades in an alkaline aqueous medium to *cis*-[Co^{III}L₂]³⁺. The *trans*-*cis* isomerization is remarkable because both the *cis* and *trans* isomers of [Co^{III}L₂]³⁺ are highly inert to ligand substitution.



Density Functional Theory Mechanistic Study of the Reduction of CO₂ to CH₄ Catalyzed by an Ammonium Hydridoborate Ion Pair: CO₂ Activation via Formation of a Formic Acid Entity
Mingwei Wen, Fang Huang, Gang Lu, and Zhi-Xiang Wang*

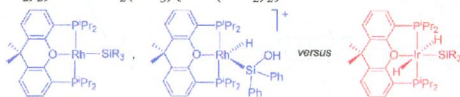
M05-2X calculations have been applied to understand the reduction mechanism of CO₂ to CH₄ catalyzed by [TMPH]⁺[HB(C₆F₅)₃]⁻ (TMP = 2,2,6,6-tetramethylpiperidine) and B(C₆F₅)₃ with silane ([Si]H) as the reductant. The CO₂ activation proceeds via formation of an intermediate in which a HCOOH entity is well formed, followed by O–H bond breaking of the HCOOH entity to transfer H^{δ-} to TMP. Unlike the CO₂ activation in the PCP-pincer nickel hydride ([Ni]H)- and N-heterocyclic carbene (NHC)-catalyzed CO₂ conversion to methanol, the direct insertion of CO₂ into the B–H bond of the catalyst is inoperative. The study elucidates why the present system can reduce CO₂ to CH₄, while the [Ni]H and NHC catalysts only can reduce CO₂ to the methoxy level.



POP-Pincer Silyl Complexes of Group 9: Rhodium versus Iridium

Miguel A. Esteruelas,* Montserrat Oliván, and Andrea Vélez

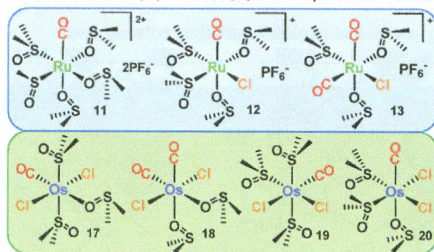
The Rh{xant(PⁱPr₂)₂} metal fragment favors unsaturated d⁸-square planar, Rh(SiR₃){xant(PⁱPr₂)₂}, and d⁶-five coordinate, [RhH{Si(OH)Ph₂}{xant(PⁱPr₂)₂}]⁺, silyl complexes, whereas the Ir{xant(PⁱPr₂)₂} metal fragment stabilizes saturated d⁶-silyl derivatives, IrHCl(SiR₃){xant(PⁱPr₂)₂} and IrH₂(SiR₃){xant(PⁱPr₂)₂}.



New Cationic and Neutral Ru(II)- and Os(II)-dmsO carbonyl Compounds

Ioannis Bratsos, Simone Calmo, Ennio Zangrando, Gabriele Balducci, and Enzo Alessio*

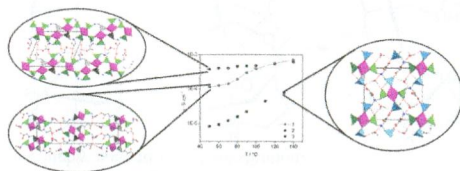
Three cationic Ru(II)-dmsO carbonyls (11–13) and of four neutral mono- and dicarbonyl Os(II)-dmsO derivatives (17–20) have been prepared and structurally characterized. By virtue of the easily replaceable dmsO ligands, they are potential well-behaved precursors for the preparation of new Ru(II) and Os(II) carbonyls.



Synthesis, Crystal Structure, and Proton Conductivity of One-Dimensional, Two-Dimensional, and Three-Dimensional Zirconium Phosphonates Based on Glyphosate and Glyphosine

Marco Taddei,* Anna Donnadio,* Ferdinando Costantino, Riccardo Vivani, and Mario Casciola

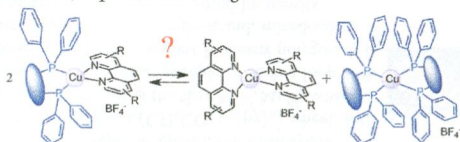
Three new zirconium phosphonates based on glyphosate and glyphosine building blocks were synthesized, and their structures were solved ab initio from XRD data (both powder and single crystal). The proton conductivities of the three materials were measured, reaching values as high as 10^{-3} S cm^{-1} , and their relationship with the crystal size and degree of hydration was studied.



Heteroleptic Copper(I) Complexes Prepared from Phenanthroline and Bis-Phosphine Ligands

Adrien Kaeser, Meera Mohankumar, John Mohanraj, Filippo Monti, Michel Holler, Juan-José Cid, Omar Moudam, Iwona Nierengarten, Lydia Karmazin-Brelot, Carine Duhayon, Béatrice Delavaux-Nicot,* Nicola Armaroli,* and Jean-François Nierengarten*

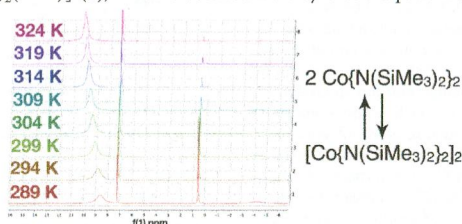
Whatever the bis-phosphine ligand, stable heteroleptic $[\text{Cu}(\text{NN})(\text{PP})]^+$ complexes are obtained from the 2,9-unsubstituted-1,10-phenanthroline ligands. By contrast, heteroleptic complexes obtained from 2,9-substituted-1,10-phenanthroline are generally stable in the solid state, but a dynamic ligand exchange reaction is systematically observed in solution, and the homoleptic/heteroleptic ratio is highly dependent on both the nature of the bis-phosphine ligand and the size of the substituents at the 2,9-positions of the 1,10-phenanthroline ligand.



Synthesis, Spectroscopic Characterization, and Determination of the Solution Association Energy of the Dimer $[\text{Co}\{\text{N}(\text{SiMe}_3)_2\}_2]_2$: Magnetic Studies of Low-Coordinate Co(II) Silylamides $[\text{Co}\{\text{N}(\text{SiMe}_3)_2\}_2\text{L}]$ (L = PMe_3 , Pyridine, and THF) and Related Species That Reveal Evidence of Very Large Zero-Field Splittings

Aimee M. Bryan, Gary J. Long,* Fernande Grandjean,* and Philip P. Power*

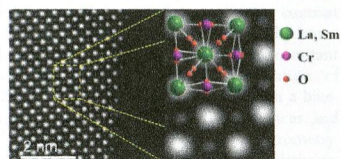
^1H NMR spectroscopy of the synthetically important paramagnetic cobalt(II) disilylamide dimer $[\text{Co}\{\text{N}(\text{SiMe}_3)_2\}_2]_2$ (**1**) in benzene solution shows that it exists in equilibrium with its monomer $\text{Co}\{\text{N}(\text{SiMe}_3)_2\}_2$ and has an association energy of -0.30 kcal mol $^{-1}$. Magnetic investigations of **1** show that the Co ions are strongly coupled antiferromagnetically. The three-coordinated Lewis base complexes formed by **1**— $[\text{Co}\{\text{N}(\text{SiMe}_3)_2\}_2\text{L}]$, where L = trimethylphosphine (PMe_3) (**2**), pyridine (**3**), and tetrahydrofuran (THF) (**4**)—display high magnetic moments with large negative D -values (between -62 cm $^{-1}$ and -82 cm $^{-1}$). The magnetic data, together with its electronic spectrum, show that earlier studies of **1** were likely made on its THF complex $[\text{Co}\{\text{N}(\text{SiMe}_3)_2\}_2(\text{THF})]$ (**4**), which is obtained if the synthesis is performed in THF.



Structures and Magnetism of the Rare-Earth Orthochromite Perovskite Solid Solution $\text{La}_x\text{Sm}_{1-x}\text{CrO}_3$

Luke M. Daniels, Mads C. Weber, Martin R. Lees, Mael Guennou, Reza J. Kashtiban, Jeremy Sloan, Jens Kreisel, and Richard I. Walton*

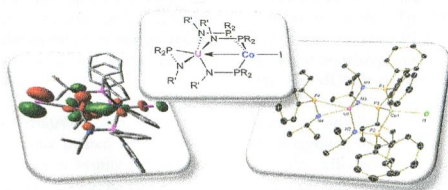
Hydrothermal synthesis at 375 °C allows the formation of a new chromite solid solution as highly crystalline and homogeneous polycrystalline powders and as evidenced by high-resolution TEM and Raman spectroscopy. Detailed studies of magnetic behavior have been performed.



Tris(phosphinoamide)-Supported Uranium–Cobalt Heterobimetallic Complexes Featuring $\text{Co} \rightarrow \text{U}$ Dative Interactions

J. Wesley Napoline, Steven J. Kraft, Ellen M. Matson, Phillip E. Fanwick, Suzanne C. Bart,* and Christine M. Thomas*

A series of U/Co heterobimetallic complexes is reported, revealing unusual metal–metal interactions between an actinide and a transition metal center.



Additions and Corrections

12178 **S**

[dx.doi.org/10.1021/ic4023807](https://doi.org/10.1021/ic4023807)

Correction to Gadolinium Acetylacetonate Tetraphenyl Monoporphyrinate Complex and Some of Its Derivatives: EXAFS Study and Molecular Dynamics Simulation

J. H. Agondanou, I. Nicolis, E. Curis, J. Purans, G. A. Spyroulias, A. G. Coutsolelos,* and S. Bénazeth*

12179

[dx.doi.org/10.1021/ic402413t](https://doi.org/10.1021/ic402413t)

Correction to Highly Reduced Double-Decker Single-Molecule Magnets Exhibiting Slow Magnetic Relaxation

Mathieu Gonidec, Itana Krivokapic, Jose Vidal-Gancedo, E. Stephen Davies, Jonathan McMaster, Sergiu M. Gorun,* and Jaume Veciana*